Presented at the XIV Masurian School
of Nuclear Physics, Mikolajki, Poland,
Aug. 31-Sept. 12, 1981.

LBL--13637

DE82 005762

ANGULAR MOMENTUM AND LINEAR MOMENTUM TRANSFER IN INTERMEDIATE-ENERGY HEAVY-ION REACTIONS

G. J. Wozniak, C. C. Hsu, D. J. Morrissey, L. W. Richardson, and L. G. Moretto

Nuclear Science Division, Lawrence Berkeley Laboratory,
University of California
Berkeley, CA 94720

This work was supported by the Director, Office of Energy Research,
Office of High Energy and Nuclear Physics
of the U.S. Department of Energy under Contract No W-7405-ENG-48

ANGULAR MOMENTUM AND LINEAR MOMENTUM TRANSFER IN INTERMEDIATE ENERGY HEAVY-ION REACTIONS*

G. J. Wozniak, C. C. Hsu,† D. J. Morrissey,‡ L. W. Richardson,** and L. G. Moretto

Nuclear Science Division, Lawrence Berkeley Laboratory,
University of California
Berkeley, CA 94720

Abstract:

In order to explore the changing role of angular momentum transfer to the heavy target-like fragment in heavy-ion reactions, the gamma-ray multiplicities associated with projectile residues were measured in the reaction of ^{20}Ne with ^{181}Ta in the energy range of 7.5 to 42 MeV/nucleon. From the gamma-ray multiplicities, the intrinsic spin of the target-like nucleus was determined and corrected for the spin removed by evaporated particles. Comparisons of the measured intrinsic spin with that expected from the missing linear momentum were found to be good at low energies but failed around a bombarding energy of 17 MeV/nucleon. From the results of these studies we infer that angular momentum and therefore linear momentum is being carried away in significant amounts by particles which were not detected.

* Research sponsored by the Nuclear Science Division of the U.S. Department of Energy under Contract W-7405-ENG-48.

† Permanent address: Institute of Atomic Energy, Beijing, China.

‡ Permanent address: Department of Chemistry, Michigan State University, East Lansing, Michigan 48824

** Present address: National Superconducting Cyclotron Laboratory, Michigan State University, East Lansing, Michigan 48824

1. Introduction

An important question regarding heavy-ion collisions is how the reaction mechanism evolves from the extensive relaxation and diffusive evolution prevailing in the low energy regime to the fragmentation processes observed in the relativistic regime. A detailed study[1] of the linear momentum transfer has demonstrated that the $^{16}O + ^{238}U$ reaction deviates from two-body kinematics at a bombarding energy of 20 MeV/A. It would be interesting to systematically study similar deviations for other reaction systems. In this paper, a complementary technique is presented for studying the two-body character of a heavy-ion reaction with nonfissioning products.

In this technique we indirectly determine the linear momentum transferred to the product nucleus by measuring the angular momentum converted into intrinsic spin via γ-ray multiplicity (M_γ) techniques. For peripheral collisions the connection between the linear and angular momenta transferred is straightforward because a localized linear impulse on the periphery of the target nucleus gives rise to a torque which causes the target nucleus to spin.[2] Measurements of the energy and angular distributions of the projectile residues and the associated $\langle M_\gamma \rangle$ for the $^{20}Ne + ^{181}Ta$ reaction allow for the determination of the amount of linear momentum transferred into the intrinsic spin of the two fragments.[3,4] This intrinsic spin can also be calculated in a simple model as a function of the detected fragment's mass and energy.

The ^{20}Ne plus ^{181}Ta system was chosen for this survey because it has several attractive features. At present ^{20}Ne is the most massive projectile available at useful intensities at the Lawrence Berkeley Laboratory (LBL) over a broad energy range (7.5-42 MeV/A). The ^{20}Ne beams at or below 22 MeV/A were obtained from the LBL 88" cyclotron. The 42 MeV/A ^{20}Ne beam was obtained at the low-energy-beam-line of the LBL Bevalac. In this energy range large amounts of entrance channel orbital angular momentum are available (80-290ħ). For low bombarding energies and very asymmetric systems, the rigid limit is approached and the intrinsic spin is concentrated in the heavy fragment. And, because the heavy products from the $^{20}Ne + ^{181}Ta$ reaction have large fission and Coulomb barriers, their intrinsic spin is carried off predominantly by the γ-ray cascade.[4])

2. Results

2.1 Particle Singles

In general terms the shape of the energy spectra of the projectile-like fragments detected at the grazing angle show simple scaling by the incident MeV/A. A typical set of such energy spectra is shown in figure 1 for nitrogen products detected at the grazing angle (solid histograms). The energy spectra are all dominated by a Gaussian-like peak centered below the beam velocity with a tail to low energy. More insight into the reaction processes can be gained by examination of more complete energy and angular distributions. In figures 2, 3 and 4, Wilczynski-type diagrams[5]) are shown for oxygen products from reactions at 10, 17 and 42 MeV/A, respectively. The

qualitative features observed in Wilczynski diagrams for low energy reactions[5]) are a strong maximum at the grazing angle with a tail towards smaller angles and energies. For some systems this tail wraps around through zero degrees, indicating that the fragments emerge from the far side of the target nucleus.

Although the Wilczynski diagrams obtained in this work are not complete, they do contain significantly more information than the energy spectra of figure 1. At the lower bombarding energies the shapes of the cross section contours, figures 2 and 3, are fairly suggestive of a ridge which runs from the maximum towards zero degrees and then back away from zero at near Coulomb energies. The measured data at 42 MeV/A appear consistent with expectations based on systematics obtained in the low energy regime.

2.2 Particle-Gamma-Ray Coincidences

The raw gamma-ray coincidence data was first converted to average gamma-ray multiplicities as a function of the projectile residue atomic number and kinetic energy. The results for nitrogen products, which are typical, are shown by the dashed histograms along with the energy spectra in figure 1. (The $\langle M_\gamma \rangle$ histogram is fairly coarse because the coincidence efficiency was approximately 0.3 (~10 gamma-rays and $d\Omega \approx 0.03$ of 4π).) Two trends can be seen (a) $\langle M_\gamma \rangle$ increases as the energy of the projectile fragment decreases at all bombarding energies, and (b) the slope of the $\langle M_\gamma \rangle$ versus energy decreases as the bombarding energy increases. (The small amount of data shown in figure 2E

for 31 MeV/nucleon has very large error bars and is not inconsistent with these observations.)

Quantitative results on the intrinsic spin require the determination of $\langle I_{TOTAL} \rangle$ from $\langle M_\gamma \rangle$. The intrinsic spin of the two nascent fragments is obtained in a two step calculation. It is assumed that $\langle I_{TOTAL} \rangle$ represents the sum of the average spin carried off by gamma-rays, $\langle I_\gamma \rangle$, and the average spin carried off by neutrons and charged particles, $\langle I_\nu \rangle$, which preceed the gamma-ray cascade, thus:

$$\langle I_{TOTAL} \rangle = \langle I_\gamma \rangle + \langle I_\nu \rangle \quad . \tag{1}$$

If the fragments are in thermal equilibrium then some simplifying assumptions can be made. The excitation energy of a thermally equilibrated complex divides in proportion to the mass fraction, so the Ta-like fragment will get 90 percent of the excitation energy and having a high atomic number will preferentially deexcite by neutron emission but not by fission. The correction (I_ν) for the angular momentum carried away by neutrons were done following the prescription described in Ref. 6. The average spin carried off by the gamma-ray cascade can be written as:

$$\langle I_\gamma \rangle = 2[\langle M_\gamma \rangle - (N_H + N_L)] \tag{2}$$

where N_H and N_L are the numbers of statistical gamma-rays emitted by the heavy and light fragments, respectively. N_H was taken from a

recent study of continuum gamma-rays emitted by deep-inelastic rare-earth nuclei[3]) and N_L was taken to be one.

The extracted values of $\langle I_{TOTAL} \rangle$ are shown as a function of TKEL for a representative Z-value (Z = 7) in figure 5. The maximum value of $\langle I_{TOTAL} \rangle$ remains surprisingly constant over the range of bombarding energies covered. In general the value of $\langle I_{TOTAL} \rangle$ always lies between ~5 and ~50ħ and increases monotonically with TKEL. The dependence of the total intrinsic spin on TKEL is not identical at all bombarding energies. A clear decrease in slope is observed as the bombarding energy increases.

3. Model

In order to determine if the decrease in slope observed in Fig. 5 is significant, we utilized a simple model to estimate the dependence of the spin transfer on TKEL. In developing a simple model of the spin generated in the fragments by the collision process, it is important to recognize several important features of the overall product distributions and build the model around these features. The reaction cross section is concentrated in products with masses less than or equal to that of the projectile; the cross sections for products larger than the projectile are depressed by orders of magnitude. Also, as we noted above, the light products emerge with velocities peaked at values only slightly below that of the projectile. These facts suggest that these collisions are occurring on the periphery of the two nuclei. The intrinsic spin, I, that would be created by a highly localized tangential force at the nuclear surface can be estimated rather simply:

the torque, τ, is equal to the time integral of the force, F(t) crossed into the radius at which it acts:

$$\tau = \int R(t) \times F(t)\, dt \quad . \tag{3}$$

If the force is tangential and sharply peaked at some radius, $\bar{R}$, then the integral can be replaced by: $\tau = \bar{F}\ t\ \bar{R}$, where $\bar{F}$ is an average force. The connection to linear momentum balance is now obvious because the linear impulse, Δp, can be written as:

$$\Delta p = \int F(t)\, dt \quad . \tag{4}$$

For a localized force, $\Delta p = \bar{F}t$, the angular momentum is the change in linear momentum times the average radius at which it is created, $I = \Delta p \bar{R}$.

A similar analysis with the explicit matching of the entrance channel orbital angular momentum to that in the exit channel has been suggested as a tool for the analysis of light-ion reactions[2]). Assuming that the obital angular momentum is completely aligned in the entrance and exit channels, we can write a classical expression for the transferred spin:

$$L_i = L_f + \langle I_{TOTAL} \rangle \tag{5}$$

in terms of the orbital angular momenta in the entrance and exit

channels, L_i and L_f, respectively. These orbital angular momenta are calculated from the kinetic energies:

$$TKE_i = E_{12}^{Coulomb} + \frac{L_i^2\hbar^2}{2\,\mu_{12}\,R_{12}^2} \tag{6a}$$

and

$$TKE_f = E_{34}^{Coulomb} + \frac{L_f^2\hbar^2}{2\,\mu_{34}\,R_{34}^2} \tag{6b}$$

where

$$E_{jk}^{Coulomb} = \frac{Z_jZ_ke^2}{R_{jk}} \text{ and } \mu_{jk} = \frac{A_jA_k}{A_j + A_k} \quad . \tag{6c}$$

Equations 6a and 6b can be solved for the orbital angular momenta and substituted into equation 5 creating an equation for the internal spin as a function of TKEL (TKEL = 6a - 6b) and the radii R_{12} and R_{34}. Continuing in the spirit of producing an estimate of the behavior of the total intrinsic spin as a function of TKEL and bombarding energy rather than a precise theory of spin transfer, the interaction was assumed to occur at a radius given by:

$$R_{ij} = R_i + R_j + c \quad . \tag{7}$$

The individual radii, R_i etc. were taken to be effective sharp radii from the proximity model.[7] The parameter c represents the overlap

necessary for the interaction. This crude picture of the spin transfer has several deficiencies which become obvious upon application of the model to realistic cases. In the limit that excitation of the normal modes of the very asymmetric dinuclear complex[8]) is not important (low temperatures) and the angular momenta remain aligned, the shape of the variation of $\langle I_{TOTAL} \rangle$ with TKEL should be contained in our picture.

4. Discussion

The strong as well as the weak points of our picture of the spin transfer can be seen in figure 6 where the observed value of the total intrinsic spin is plotted against the value calculated from the TKEL. The single adjustable parameter, c, was set to 1 fm. The various curves seen in figure 5 fall into only two classes in figure 6 according to bombarding energy. The spin transfer is nearly equal to the simple estimate at low bombarding energies (7.5, 10) and roughly only half that at higher energies ($\geq$17). Perfect agreement between the model and experiment would, of course, yield a straight line with a slope equal to one and an intercept of (0,0). However, the discrepancies may be more apparent than significant in light of the simplicity of the model. At the lowest bombarding energies figure 6 shows a small discrepany between the model and the data, the slope is ~0.8 rather than 1. There is a dramatic decrease in the slope at 17 MeV/nucleon which is also observed at higher bombarding energies. At 17 MeV/A and above the spin transfer is less than half of that observed at lower

energies for the same product at the same energy loss and at the grazing angle.

Two possible sources of the dramatic decrease in the observed spin transfer relative to the calculated one are (a) the breakdown of the assumption that the initial reaction is "two-body," i.e. the missing projectile mass is not completely transferred to the target or (b) the breakdown of the assumption that the heavy partner remains intact and converts the angular momentum primarily into gamma-rays (no fission decay). The plausibility of the latter, that the heavy nucleus is fissioning most of the time at the higher bombarding energies, can be checked by estimating the fission to neutron emission competition as a function of spin and energy loss. At low spins the rotating liquid drop fission barriers for nuclei near tantalum are approximately 20 MeV[9]) compared to neutron binding energies of approximately 8 MeV[10]) which effectively prohibits fission. Real competition between neutron emission and fission only occurs for neutron deficient nuclei at high spins ~60ħ because only then does the fission barrier decreases to values near those of the neutron binding energies.[11])

Therefore, in light of the rejection of the fission hypothesis and the previous results of Back et al.[1]) on incomplete momentum transfer at 20 MeV/A, the former source for the discrepancy seems most likely. The simple model that we have used is based on momentum balance between the entrance and exit channels where both channels were assumed to have only "two bodies." However, if an excited projectile residue breaks up into two or more bodies then this simple

model will overestimate the spin transfer, because it assumes all missing momentum has been captured by the target nucleus.

This work was supported by the Director, Office of Energy Research, Office of High Energy and Nuclear Physics of the U.S. Department of Energy under Contract No W-7405-ENG-48.

References

1. B. B. Back, K. L. Wolf, A. C. Mignerey, C. K. Gelbke, T. C. Awes, H. Breuer, V. E. Viola, Jr., and P. Dyer, Phys. Rev. C22 (1980) 1927, and P. Dyer, et al., Phys. Rev. Lett. 42 (1979) 560.
2. D. M. Brink, Phys. Lett. 40B (1972) 37.
3. R. J. McDonald, A. J. Pacheco, G. J. Wozniak, L. G. Moretto, C. Schuck, S. Shih, R. M. Diamond, and F. S. Stephens, Nucl. Phys. in press (1981).
4. R. M. Diamond and F. S. Stephens, Annl. Rev. Nucl. Part. Sci. 30 (1980) 85.
5. J. Wilczynski, Phys. Lett. 47B (1973) 484.
6. S. K. Blau and L. G. Moretto, Nucl. Phys. A 359 (1981) 477.
7. J. Blocki, J. Randrup, W. J. Swiatecki and C. F. Tsang, Annl. Phys. 105 (1977) 427.
8. L. G. Moretto and R. P. Schmitt. Phys. Rev. C21 (1980) 204.
9. S. Cohen, F. Plasil and W. J. Swiatecki, Annl. Phys. 82 (1974) 557.
10. A. H. Wapstra and K. Bos, Atomic Data and Nucl. Data Tables 17 (1976) 474.
11. H. C. Britt, B. H. Erkkila, P. D. Goldstone, R. H. Stokes, B. B. Back, F. Folkmann, O. Christensen, B. Fernandez, J. D. Garrett, G. B. Hagemann, B. Herskind, D. L. Hillis, F. Plasil, R. L. Ferguson, M. Blann and H. H. Gutbrod, Phys. Rev. Lett. 39 (1977) 1458.

Figure Captions

Figure 1. A comparison of the general features of the energy spectra (solid curves) and the gamma-ray multiplicity (dashed curves) for nitrogen products detected near the grazing angle is shown as a function of bombarding energy.

Figure 2. Wilczynski-type diagram for oxygen products from the reaction of 10 MeV/nucleon ^{20}Ne with ^{181}Ta. The dashed curve labeled V_C^{Lab} represents the kinetic energy of oxygen fragments with only the Coulomb energy (calculated for rigid spheres separated by 2 Fermis.)

Figure 3. Similar to figure 2, oxygen products from the reaction of 17 MeV/nucleon ^{20}Ne with ^{181}Ta.

Figure 4. Similar to figures 2 and 3, oxygen products from the reaction of 42 MeV/nucleon ^{20}Ne with ^{181}Ta.

Figure 5. The extracted total spin $\langle I_{TOTAL} \rangle$ is shown as a function of TKEL for nitrogen products from reactions at 7.5, 10, 17, 22 and 42 MeV/nucleon, from top to bottom in the figure. Solid lines are drawn through the data to emphasize the differences in slope.

Figure 6. The total spin $\langle I_{TOTAL}^{CALC} \rangle$ calculated from the TKEL is plotted against the total spin $\langle I_{TOTAL}^{OBS} \rangle$ extracted from $\langle M_\gamma \rangle$. Perfect agreement would give a slope of 1, the grouping of the data by the bombarding energy is discussed in the text.

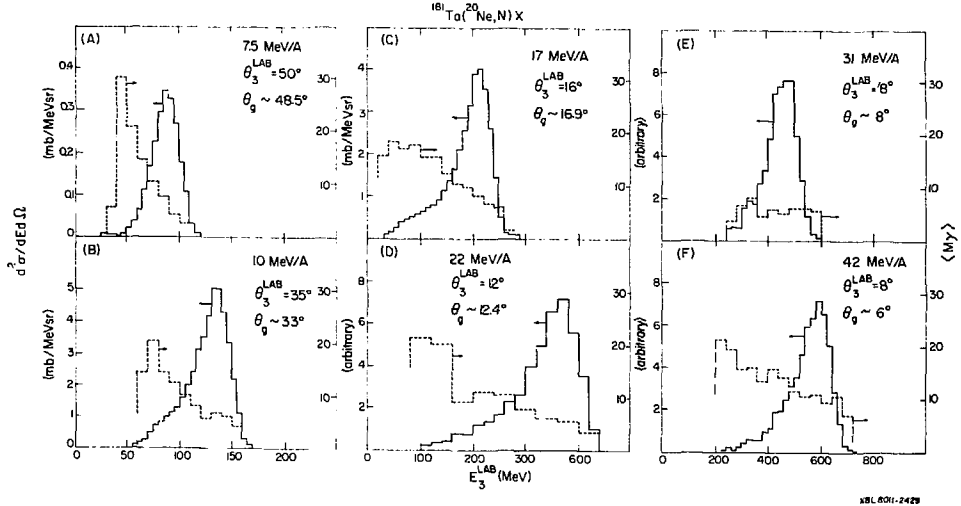
^{181}Ta(^{20}Ne,N)X
(A)
7.5 MeV/A
θ_3^{LAB}=50°
θ_g ~ 48.5°
(B)
10 MeV/A
θ_3^{LAB}=35°
θ_g ~ 33°
(C)
17 MeV/A
θ_3^{LAB}=16°
θ_g ~ 16.9°
(D)
22 MeV/A
θ_3^{LAB}=12°
θ_g ~ 12.4°
(E)
31 MeV/A
θ_3^{LAB}=8°
θ_g ~ 8°
(F)
42 MeV/A
θ_3^{LAB}=8°
θ_g ~ 6°
$d^2\sigma/dEd\Omega$
(mb/MeVsr)
(arbitrary)
$\langle My \rangle$
E_3^{LAB} (MeV)
XBL 801-2429

Fig. 1

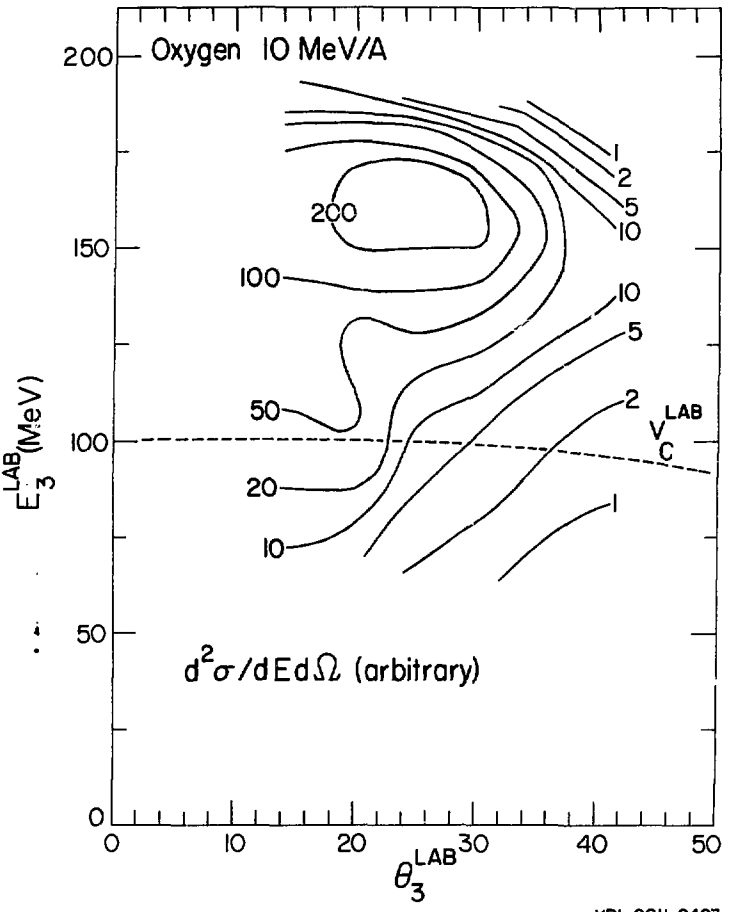
Oxygen 10 MeV/A
200
150
100
50
0
0
10
20
30
40
50
E_3^{LAB}(MeV)
θ_3^{LAB}
200
100
50
20
10
1
2
5
10
10
5
2
1
V_C^{LAB}
$d^2\sigma/dEd\Omega$ (arbitrary)
XBL 8011-2423

Fig. 2

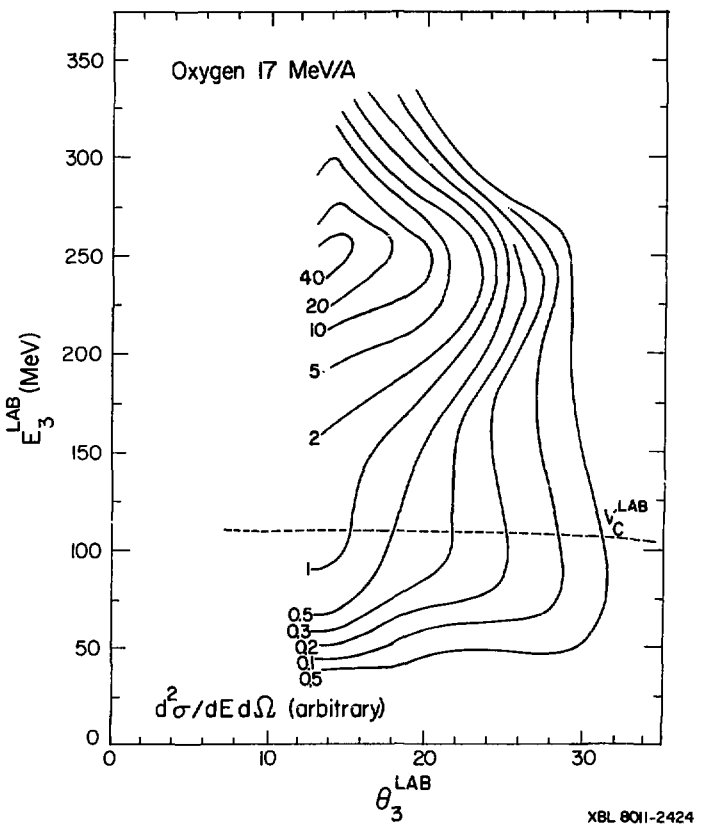
Oxygen 17 MeV/A
350
300
250
200
150
100
50
0
0
10
20
30
E_3^{LAB} (MeV)
θ_3^{LAB}
V_C^{LAB}
40
20
10
5
2
1
0.5
0.3
0.2
0.1
0.5
$d^2\sigma/dE\,d\Omega$ (arbitrary)
XBL 8011-2424

Fig. 3

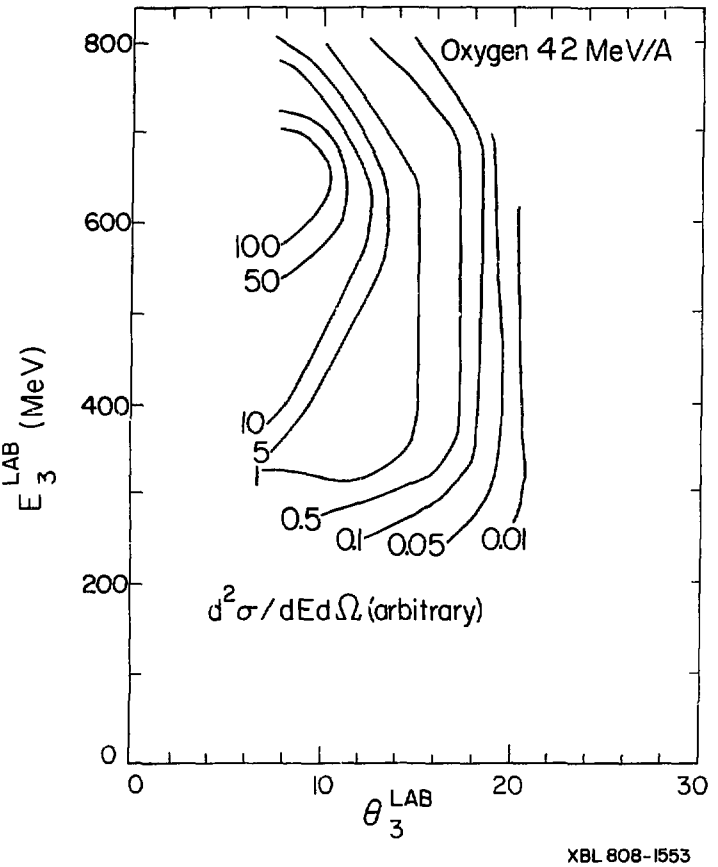
Oxygen 42 MeV/A
800
600
400
200
0
0
10
20
30
E_3^{LAB} (MeV)
θ_3^{LAB}
100
50
10
5
1
0.5
0.1
0.05
0.01
$d^2\sigma/dEd\Omega$ (arbitrary)
XBL 808-1553

Fig. 4

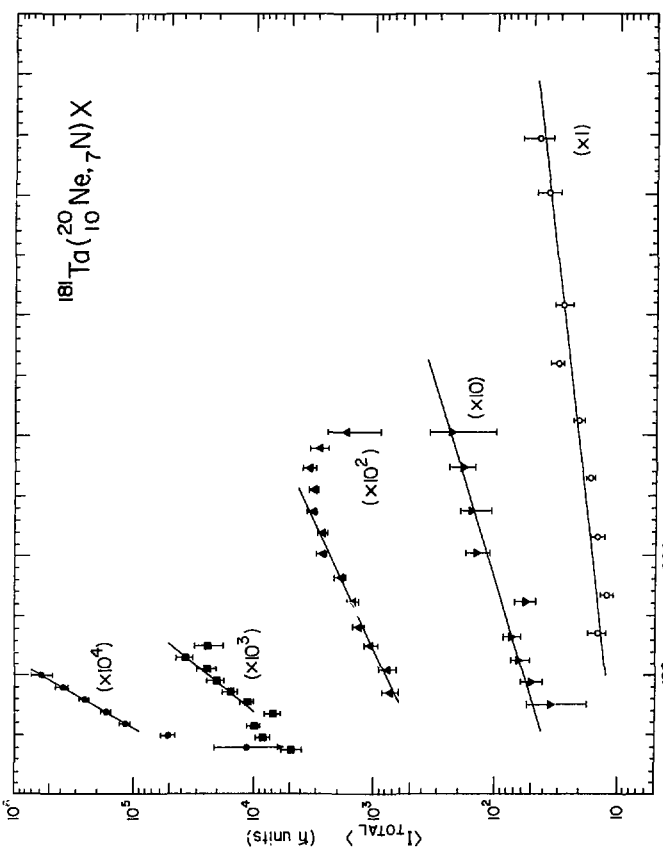
$^{181}Ta(^{20}_{10}Ne,_{7}N)X$
(×10⁴)
(×10³)
(×10²)
(×10)
(×1)
⟨I_TOTAL⟩ (ħ units)
TKEL (MeV)
XBL-812-173

Fig. 5

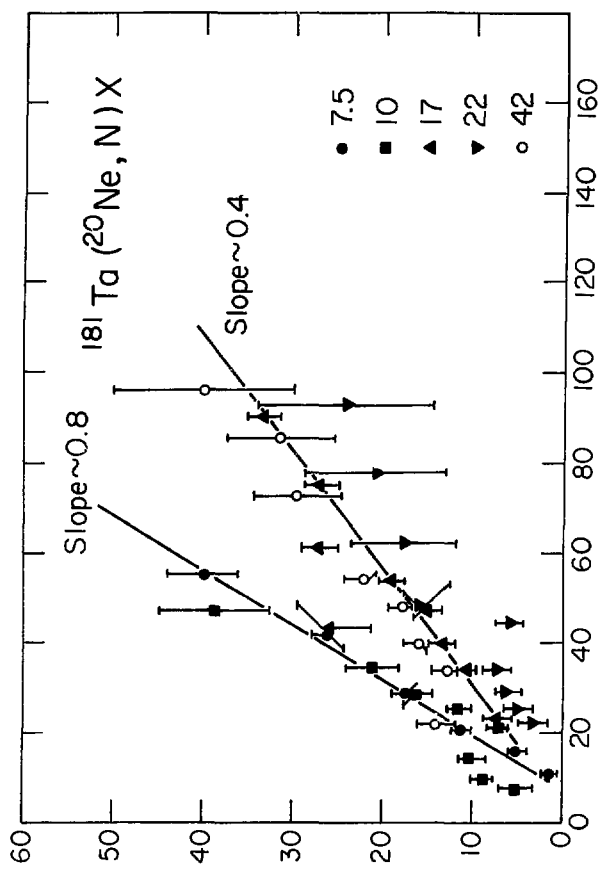

XBL818-2426

Fig. 6